Method for determining full-field absolute phases in the common-path heterodyne interferometer with an electro-optic modulator

Yen-Liang Chen and Der-Chin Su*

Department of Photonics and Institute of Electro-Optical Engineering, National Chiao-Tung University, 1001 Ta-Hsueh Road, Hsinchu 30050, Taiwan

*Corresponding author: t7503@faculty.nctu.edu.tw

Received 11 July 2008; revised 31 October 2008; accepted 4 November 2008; posted 4 November 2008 (Doc. ID 98663); published 3 December 2008

When a sawtooth voltage signal with the amplitude lower than its half-wave voltage is applied to drive an electro-optic modulator, the interference signals become a group of periodic sinusoidal segments. A new algorithm is proposed to modify these segments to an associated continuous sinusoidal wave, and then its initial phase can be determined. Subtracting the characteristic phase of the modulator from the initial phase, the absolute phase can be obtained. This technique is applied to all pixels, and full-field absolute phase measurements can be achieved. The validity of this method is demonstrated. © 2008 Optical Society of America

OCIS codes: 230.2090, 040.2840, 120.5050, 120.3180.

1. Introduction

In heterodyne interferometry [1–5], the measured absolute phase is the phase difference between the test signal and the reference signal. The reference signal can be obtained with a light signal drawn from a beam splitter or an electronic signal directly introduced from an electronic device. In general, it is a high-resolution technique for one-point measurement. However, as it extends to the full-field measurements, the measurement processes become tedious due to the time-consuming two-dimensional scanning involved. Consequently, it is necessary to develop a convenient full-field heterodyne interferometry with a fast camera to grab the discrete digital signals in a limited exposure time. Although Jian *et al.*[6] proposed an optimal condition for full-field heterodyne interferometry, the recorded test signals had uncertain time differences with respect to the commonly used reference signals. Hence, it was difficult to measure the full-field absolute phases. In several papers, methods to overcome this problem have been proposed [7–10]. They are also valid only for the relative phase measurements with the exception of Akiba's method [10]. In Akiba's method, a pair of cameras is used to take two images simultaneously, and it is difficult to make these two images match each other very well.

In this paper, a novel method for determining full-field absolute phases in the common-path heterodyne interferometer is proposed by modifying Chiu's method [5]. Chiu's method has good measurement results, but it is suitable only for one-point measurement. Although both of them need an electro-optic modulator driven with a sawtooth voltage signal, the amplitude is lower than its half-wave voltage in this method instead of the half-wave voltage in Chiu's method. In addition, a fast camera is introduced to replace the photodetector, and the reference signals in Chiu's method are not suitable for this method. Then, a group of periodic sinusoidal segments at every pixel is obtained. In the full-field measurements, these segments are taken by a fast camera and become discrete digital signals. After a series of operations, the starting point of the sampled

0003-6935/08/356518-06$15.00/0

sinusoidal segment can be determined accurately. Next, the period of the sampled sinusoidal segments is lengthened, and the segments can be modified to a continuous sinusoidal wave by using a least-square sine fitting algorithm [11]. The initial phase of the continuous sinusoidal wave can also be estimated. Subtracting the characteristic phase of the modulator from the initial phase, the absolute phase measured at the pixel can be obtained. These operations are applied to other pixels, and full-field absolute phase measurements can be achieved. The validity of this method is demonstrated.

2. Principle

A. Waveforms of the Interference Signals

Figure 1 shows the optical configuration of a conventional common-path heterodyne interferometer with an electro-optic modulator for one-point measurement [5]. For convenience, the $+z$ axis is chosen along the propagation direction and the y axis is along the vertical direction. Its heterodyne light source (HLS) consists of a linearly polarized laser (LS), an electro-optic modulator (EO) with half-wave voltage V_π, a voltage linear amplifier (VLA), and a function generator (FG). A linearly polarized light at 45° with respect to the x axis passes through the EO with the axis at 0° with respect to the x axis under an applied field. An external sawtooth voltage signal with a moderate dc bias coming from the FG and the VLA is applied to the EO. If its period and amplitude are T and V, respectively, then the phase retardation between the s and the p polarizations can be given as [12]

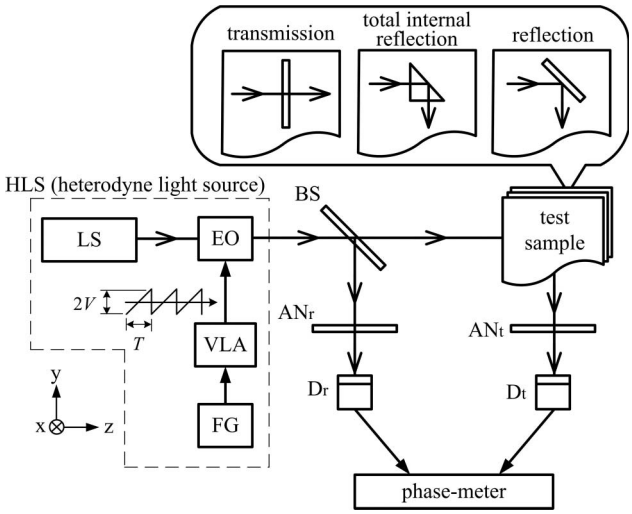

Fig. 1. Schematic diagram for the common-path heterodyne interferometer with an electro-optic modulator: LS, laser light source; EO, electro-optic modulator; FG, function generator; VLA, voltage linear amplifier; BS, beam splitter; AN, analyzer; D, photodetector.

$$\Gamma = \frac{\pi}{V_\pi} V_z = \frac{\pi}{V_\pi}\left[\frac{2V}{T}(t - mT) - V\right] = 2\pi \frac{V}{V_\pi T}(t - mT) - \phi_0, \tag{1}$$

where the characteristic phase $\phi_0 = (V/V_\pi)\pi$, $mT \le t \le (m+1)T$, and m is an integer. After the light beam passes through (or is reflected by) the test sample, there is an additional phase difference φ between the s and the p polarizations. Then, it passes through an analyzer AN_t and enters the photodetector D_t. The transmission axis of the AN_t is located at 45° with respect to the x axis, the test signal can be written as

$$\begin{aligned} I(t) &= \frac{1}{2}[1 + \cos(\Gamma + \phi)] \\ &= \frac{1}{2}\left\{1 + \cos\left[2\pi \frac{V}{V_\pi T}(t - mT) - \phi_0 + \phi\right]\right\} \\ &= \frac{1}{2}\left\{\left[1 + \cos\left(2\pi \frac{V}{V_\pi T} t + \psi\right)\right] \cdot \mathrm{rect}\left(\frac{t}{T} - \frac{1}{2}\right)\right\} \\ &\quad * \sum_{i=0}^{n-1} \delta(t - iT), \end{aligned} \tag{2}$$

where $\psi = \phi - \phi_0$, n is the maximum of m, and the operator rect[ ] and the symbol * represent the rectangle function and the convolution operation, respectively. In Eq. (2), it can be seen that the period of the cosine function is $V_\pi T/V$; both the window width of the rectangle function and the period of the windowed delta function are T. In the conventional tests, the condition $V = V_\pi$ is chosen, Eq. (2) can be rewritten as

$$I(t) = \frac{1}{2}\left[1 + \cos\left(2\pi \frac{t}{T} + \psi\right)\right], \tag{3}$$

and $I(t)$ becomes a continuous sinusoidal signal. In general, the reference signal coming from the photodetector D_r or the FG always has the form

$$I_r(t) = \frac{1}{2}\left(1 + \cos 2\pi \frac{t}{T}\right). \tag{4}$$

The data of ψ can be easily obtained by comparing the test signal and the reference signal in a phase meter or a lock-in amplifier.

On the other hand, the optical configuration should be modified as shown in Fig. 2 for full-field measurements. A microscopic objective (MO), a pinhole (PH), and a collimating lens (CL) are added to expand and collimate the light beam. The transmission axis of the AN is still located at 45° with respect to the axis, and a fast complimentary metal oxide semiconductor (CMOS) camera is used to replace the D_t. Because the two-dimensional sampled interference signals in a limited recording time are taken,

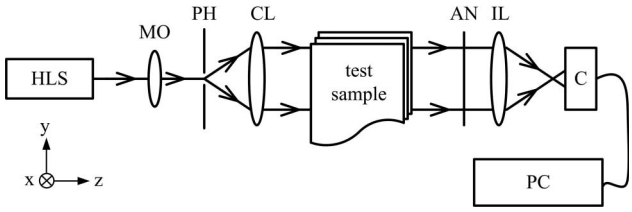

Fig. 2. Schematic diagram for the full-field common-path heterodyne interferometer: HLS, heterodyne light source; MO, microscopic objective; PH, pinhole; CL, collimating lens; AN, analyzer; IL, imaging lens; C, CMOS camera; PC, personal computer.

there is an uncertain time discrepancy between the sampled interference signals at each pixel and the signal coming from the D_t or the FG. Consequently, it is difficult to get the data of ψ at each pixel with conventional techniques. If the condition $V < V_\pi$ occurs, the period of cosine function in Eq. (3) is longer than T. $I(t)$ becomes a group of periodic sinusoidal segments, and each segment has an initial phase ψ. For clarity, the interference signal as V is changed from 80 V to 120 V with 20 V steps under $\psi = 60°$ and the following experimental condition:$V_\pi = 148$ V are depicted and shown in Fig. 3(a). If both the window width of the rectangle function and the period of the windowed function are lengthened to $(T + \Delta t)$, Eq. (2) can be expressed as

$$I_c(t) = \frac{1}{2}\left\{\left[1 + \cos\left(2\pi \frac{V}{V_\pi T} t + \psi\right)\right] \cdot \mathrm{rect}\left(\frac{t}{T + \Delta t} - \frac{1}{2}\right)\right\} * \sum_{i=0}^{n-1} \delta[t - i\,(T + \Delta t)], \tag{5}$$

where $T + \Delta t = V_\pi T/V$. Consequently, the interference signals shown in Fig. 3(a) are modified and become the waveforms, as shown in Fig. 3(b). It can be seen that these waveforms are continuous sinusoidal signals with different periods. If ψ can be measured accurately, the data of φ can be calculated under the condition V and V_π are specified.

B. Algorithm for Determining Absolute Phases

When a fast CMOS camera is used to record the interference signals under the condition $V < V_\pi$, the discrete digital signals taken at each pixel are shown in Fig. 4. The symbol • indicates the sampling positions. The theoretical starting points of sinusoidal segments in the time axis are at local extreme positions, which can be determined by operating the second order differential on Eq. (2). They are always different from the sampled starting points of the discrete digital signals taken by a camera. In theory, the ending point of one segment coincides with the starting point of the next segment. However, the sampled starting point of every segment may not be at the same relative position and may not be at the theoretical starting point of the associated segment. To determine an "optimum segment" whose sampled starting point is located closest to the theoretical starting point of the associated segment, let P_m and C_m be the sampled starting point and the time comparing point of the mth segment, respectively, and the initial condition $C_1 = P_1$ exist. Then, the conditions

$$C_{m+1} = C_m + T, \quad \text{if } P_{m+1} > C_m + T\ , \tag{6-1}$$

$$C_{m+1} = P_{m+1}, \quad \text{if } P_{m+1} \le C_m + T. \tag{6-2}$$

should be applied iteratively until the optimum segment has been identified, where $m = 1, 2, 3, \ldots, i$.

For clarity, the conditions for Eqs. (6-1) and (6-2) are shown in Figs. 4(a) and 4(b), respectively. If the ith segment is the optimum segment, then the time axis is so shifted that the condition $P_i = 0$ is given and it can be written as

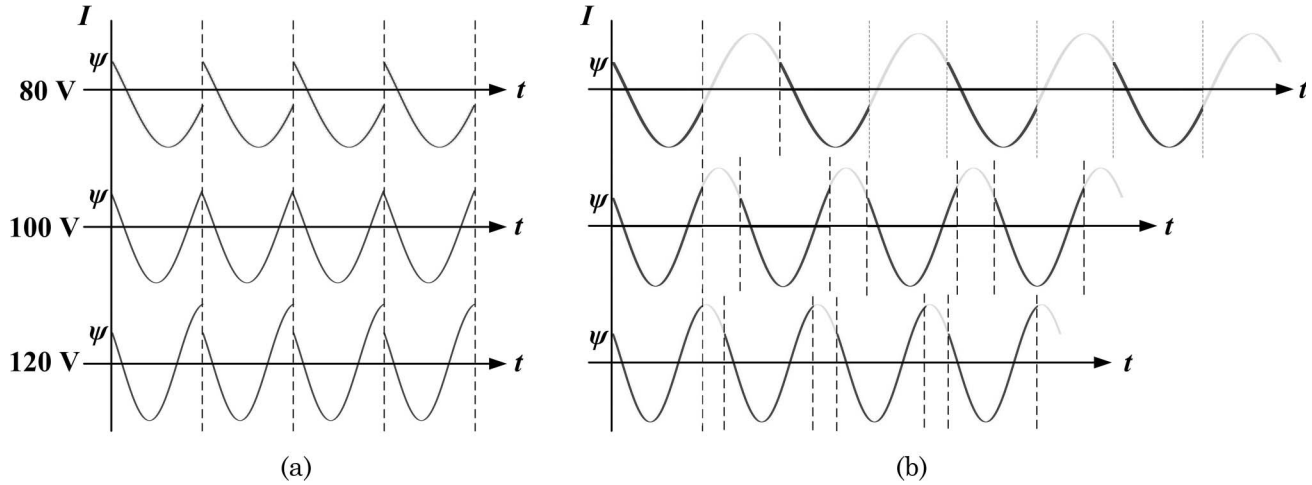

Fig. 3. (a) Interference signals as V is changed from 80 V to 120 V with 20 V steps under the conditions $V_\pi = 148$ V and $\psi = 60°$. (b) Corresponding modified interference signals with lengthened periods.

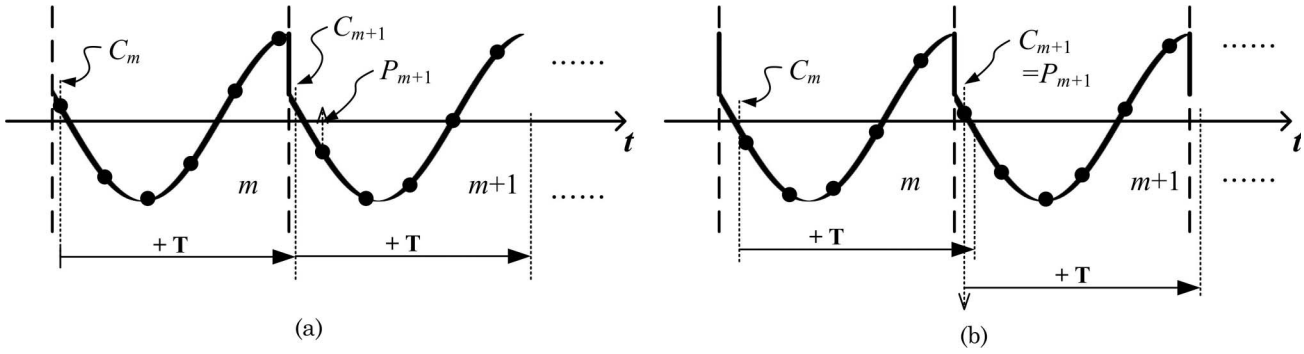

Fig. 4. The conditions are applied to identify the optimum segment as (a) $P_{m+1} > C_m + T$ and (b) $P_{m+1} \le C_m + T$.

$$I_i(t) = \frac{1}{2}\left\{\left[1 + \cos\left(2\pi\frac{V}{V_\pi T}t + \psi\right)\right] \cdot \mathrm{rect}\left(\frac{V}{V_\pi T}t - \frac{1}{2}\right)\right\} * \sum_{g=0}^{h-1}\delta\left(t - \frac{g}{f_s}\right), \quad (7)$$

where g is a positive integer and f_s and h are the sampling frequency and the number of sampled points in the ith segment, respectively. Next, the period difference $\Delta t = (V_\pi - V)T/V$ is inserted into any two consecutive sampled segments where $m \ge i$, as shown in Fig. 5. Based on the operations with the least-square sine fitting algorithm [11], these sampled segments can be modified to a continuously sinusoidal wave that can be expressed as

$$I_c(t) = \frac{1}{2}\left[1 + \cos\left(2\pi\frac{V}{V_\pi T}t + \psi\right)\right] = A \cdot \cos\left(2\pi\frac{V}{V_\pi T}t\right) + B \cdot \sin\left(2\pi\frac{V}{V_\pi T}t\right) + C. \quad (8)$$

Here, A, B, and C are real numbers and ψ can be determined with the equation

$$\psi = \tan^{-1}\left(\frac{-B}{A}\right). \quad (9)$$

Consequently, the absolute phase ϕ can be calculated under the condition that ϕ_0 is specified. For easy understanding, a flowchart for describing the whole processes is summarized and shown in Fig. 6.

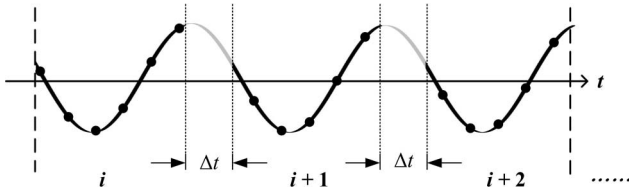

Fig. 5. Inserting Δt into any two consecutive segments.

3. Experiments and Results

To demonstrate the feasibility of this method, the full-field absolute phase retardations of a quarter-waveplate were measured. An He–Ne laser with 632.8 nm wavelength, an EO modulator (New Focus/Model 4002) with $V_\pi = 148$ V, and a CMOS camera (Basler/A504K) with 8 bit gray level and 200×200 pixels were used. Under the conditions $T = 1$ s, $V = 120$ V, sampling frequency $f_s = 45.1$ frames/s, and 500 frames were taken. The intensities of the sampled signals at the pixel $(+100, +100)$ are shown in Fig. 7. The average phase retardation of the

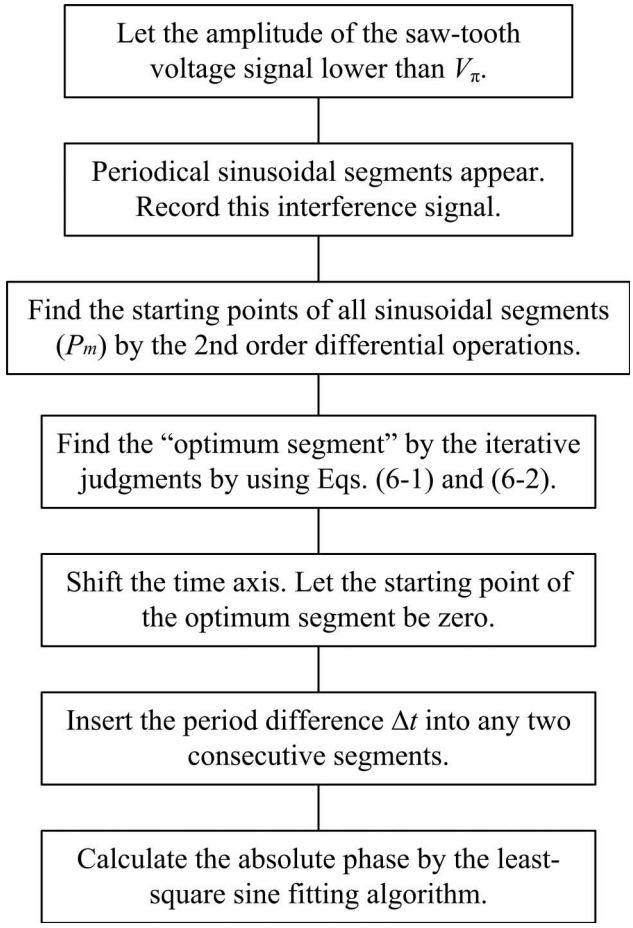

Fig. 6. Flowchart for describing the whole process.

full-field distribution and its standard deviation are 89.9° and 0.7°, respectively.

4. Discussion

To avoid aliasing, the condition $\Delta t < T$ should be valid according to the Nyquist sampling theorem [13]. So this method is easily operated under the condition $(V_\pi/2) < V < V_\pi$, and the condition $V \approx (3V_\pi/4)$ was chosen in our experiments. Moreover, if F_s is a multiple of $1/T$, then each segment has the same sampled points. Consequently, Eq. (6-1) and (6-2) are not valid for determining the optimum segment. The errors in the absolute phase measurements in this method may be influenced by the following factors:

1. Characteristic phase error

The errors in V and V_π directly introduce a systematic error $\Delta\phi_0$ to the characteristic phase ϕ_0. The resolution of V from the power supplier is $\Delta V_1 = 0.016\,\mathrm{V}$. Also V_π can be measured [14], and its error is estimated $\Delta V_2 = 0.015\,\mathrm{V}$. Hence the maximum error of ϕ_0 can be estimated and expressed as $\Delta\phi_0 = \phi_{\max} \cdot [(\Delta V_1/V)^2 + (\Delta V_2/V_\pi)^2]^{1/2} \approx 0.03°$, where $\phi_{\max} = 180°$ is the maximum possible phase.

2. Sampling error

It depends on the frequency of the heterodyne interference signal, the camera recording time, the frame period, the frame exposure time, and the number of gray levels. The phase error from the sampling processes can also be estimated and it is given $\Delta\phi_s = 0.036°$ [6].

3. Polarization-mixing error

Owing to the extinction ratio effect of a polarizer, mixing of light polarization occurs. In our experiments, the extinction ratio of the polarizer (Japan Sigma Koki, Ltd.) is 1×10^{-5}. The ratio can be estimated in advance to modify the measured results. So, the polarization-mixing error can be decreased to $\Delta\phi_p = 0.03°$ with this modification [5].

4. Noises

In practical tests, we have a lot of noises. Because of its common-path optical configuration, two interfering beams travel the same path and they have the same phase noises from the ambient motion. These phase noises will cancel out after interfering, and they do not affect the interference signals [15]. So, this method is highly stable against the ambient motion. The noises may be electronic noises. To show the validity of our algorithm, different random noise levels from 0% to 10% are added to the theoretical digital signals taken by the camera as $\psi = 45°$. Then, they are processed to derive the absolute phases. Their associated phase errors can be calculated and shown in Fig. 8. The abscissa of Fig. 8 means the ratio of the maximum amplitude of the additional random noises to the amplitude of the theoretical signals. We have almost 5% maximum random noise level in our tests, and we have $\Delta\phi_n = 0.2°$.

Consequently, our total experimental errors are $\Delta\phi = \Delta\phi_0 + \Delta\phi_s + \Delta\phi_p + \Delta\phi_n = 0.3°$. Moreover, this method can be applied to measure two-dimensional distributions of the physical quantities that are related to the phase difference between the s and the p polarizations, such as the refractive index, the complex refractive index, (n_e, n_o), the phase retardation, etc. In addition, this method can be modified and applied to the interferometers with a polarization beam splitter.

5. Conclusion

An alternative method for full-field absolute phase measurements in a heterodyne interferometer with an electro-optic modulator has been proposed in this paper. When a sawtooth voltage signal with the amplitude lower than its half-wave voltage is applied to drive the modulator, the interference signal become a group of periodic sinusoidal segments. The initial phase of each sinusoidal segment depends on the phase difference induced by the test sample. In real measurements, each segment is taken by a camera and becomes discrete digital points. The optimal starting point of the sampled sinusoidal segment is determined accurately by a series of operations. Then, the periodic sampled sinusoidal segments are modified to derive the associated continuous sinusoidal wave, and its initial phase at optimal starting point is calculated by using a least-square sine fitting algorithm. Subtracting the characteristic phase of the modulator from the initial phase, the absolute phase can be obtained. This technique is applied to all pixels, and the full-field absolute phase

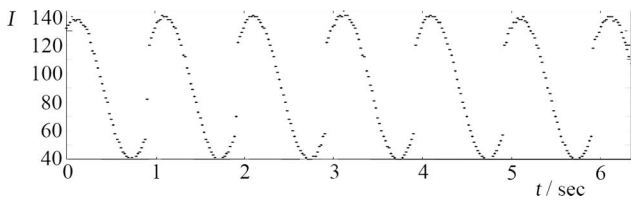

Fig. 7. Intensities of the sampled signals at the pixel $(+100, +100)$.

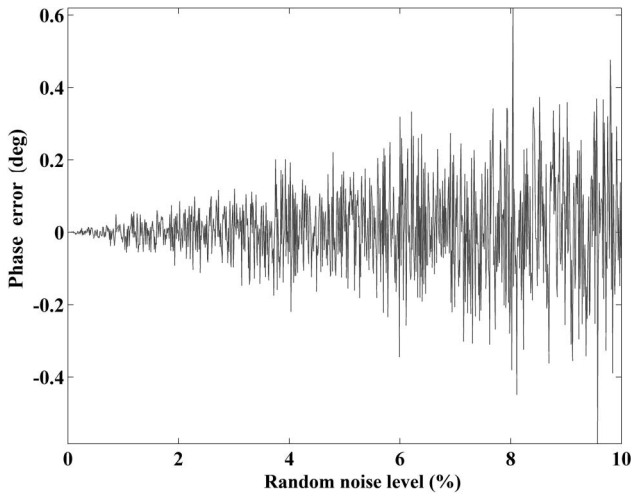

Fig. 8. Relation curves of phase error versus random noise level as $\psi = 45°$.

measurements can be achieved. Its validity has been demonstrated.

This study was supported in part by the National Science Council of Taiwan (NSCT) under Contract NSC94-2215-E-009-002.

References

1. N. A. Massie, R. D. Nelson, and S. Holly, "High-performance real-time heterodyne interferometry," Appl. Opt. **18**, 1797–1803 (1979).
2. R. Dandliker, R. Thalmann, and D. Prongue, "Two-wavelength laser interferometry using superheterodyne detection," Opt. Lett. **13**, 339–341 (1988).
3. E. Gelmini, U. Minoni, and F. Docchio, "Tunable, double-wavelength heterodyne detection interferometer for absolute-distance measurements," Opt. Lett. **19**, 213–215 (1994).
4. C. M. Feng, Y. C. Huang, J. G. Chang, M. Chang, and C. Chou, "A true sensitive optical heterodyne polarimeter for glucose concentration measurement," Opt. Commun. **141**, 314–321 (1997).
5. M. H. Chiu, J. Y. Lee, and D. C. Su, "Complex refractive-index measurement based on Fresnel's equations and uses of heterodyne interferometry," Appl. Opt. **38**, 4047–4052 (1999).
6. Z. C. Jian, Y. L. Chen, H. C. Hsieh, P. J. Hsieh, and D. C. Su, "Optimal condition for full-field heterodyne interferometry," Opt. Eng. **46**, 115604 (2007).
7. T. Tkaczyk and R. Jozwicki, "Full-field heterodyne interferometer for shape measurement: experimental characteristics of the system," Opt. Eng. **42**, 2391–2399 (2003).
8. M. C. Pitter, C. W. See, and M. G. Somekh, "Full-field heterodyne interference microscope with spatially incoherent illumination," Opt. Lett. **29**, 1200–1202 (2004).
9. P. Egan, M. J. Connely, F. Lakestani, and M. P. Whelan, "Random depth access full-field heterodyne low-coherence interferometry utilizing acousto-optic modulation and a complementary metal-oxide semiconductor camera," Opt. Lett. **31**, 912–914 (2006).
10. M. Akiba, K. P. Chan, and N. Tanno, "Full-field optical coherence tomography by two-dimensional heterodyne detection with a pair of CCD cameras," Opt. Lett. **28**, 816–818 (2003).
11. IEEE Standard 1241-2000, "Standard for terminology and test methods for analog to digital converters," (IEEE, 2000), pp. 25–29.
12. D. C. Su, M. H. Chiu, and C. D. Chen, "Simple two-frequency laser," Precis. Eng. **18**, 161–163 (1996).
13. H. Nyquist, "Certain topics in telegraph transmission theory," Trans. Am. Inst. Electr. Eng. **47**, 617–644 (1928).
14. Q. Dou, H. Ma, G. Jia, Z. Chen, K. Cao, and T. Zhang, "Study on measurement of linear electro-optic coefficient of a minute irregular octahedron cBN wafer," Opt. Laser Technol. **39**, 647–651 (2007).
15. D. Briers, "Interferometric optical testing," in *Optical Measurement Techniques and Applications*, P. K. Rastogi, ed. (Artech, 1997), pp. 101–103.